Operating regimes of a controlled dual wavelength semiconductor laser system through four-wave mixing- mediated by injection-locking

Roberts, Daniel; Pierce, Iestyn

IET Optoelectronics

DOI:
10.1049/iet-opt.2018.5019

Published: 23/10/2018

Version created as part of publication process; publisher's layout; not normally made publicly available

IET Optoelectronics

Research Article

IET Journals
The Institution of Engineering and Technology

Operating regimes of a controlled dual-wavelength semiconductor laser system through four-wave mixing- mediated by injection-locking

ISSN 1751-8768
Received on 26th April 2018
Revised 5th September 2018
Accepted on 15th October 2018
doi: 10.1049/iet-opt.2018.5019
www.ietdl.org

Daniel R.G. Roberts[1] ✉, *Iestyn Pierce*[1]

[1]*School of Computer Science and Electronic Engineering, Bangor University, Dean Street, Bangor, UK*

✉ *E-mail: d.r.g.roberts@bangor.ac.uk*

Abstract: A method of generating a non-zero frequency spacing between two laser diodes, using four-wave mixing, mediated by injection-locking in order to potentially realise THz radiation is presented. Four distinct regimes of operation are observed, including a periodic response, where the oscillations are simply related to the relaxation oscillations of the system; a periodic response with multiple frequency components, where there is a harmonic relationship between the fundamental frequency and the other frequency components; a chaotic response, where the apparent frequency components are not harmonically related; and finally the locking condition between the lasers, where a continuous wave operation is apparent. A clear linear relationship between the frequency offset and the detuning frequency while operating under the locking condition is observed, and there is a clear transition in behaviour on either side of the locking region, where the system shows a nonlinear behaviour. For higher injection rates, locking is only observed at either end of the locking region, and from this arises a so-called generalised locking region.

1 Introduction

This study will investigate a method of generating a non-zero frequency spacing between two laser diodes, using four-wave mixing (FWM) mediated by injection locking in a third laser. Using this method could lead to a potential means of efficiently generating terahertz (THz) radiation within the so-called 'THz gap' (100 GHz to 10 THz) [1, 2].

THz and millimetre wave (mm-waves) technologies, which are able to emit efficiently within the THz gap, have grown substantially over recent years due to the advancements which have been made in developing sources and detectors which have the ability to emit within this frequency range [3–7]. Applications include gas sensing using THz time-domain spectroscopy [4, 5] and T-ray imaging [6]. THz technology is also used for the detection of concealed explosives [1, 7].

It is well known that the THz waves have the ability to interact with numerous forms of matter, from solids to liquids and gasses. As a result, THz waves are attractive sources for applications in medical imaging or for security purposes [8–11] due to the substantial penetration depth, the waves have in certain materials, including certain plastics, ceramics, fabrics, wood, and paper [12]. Other highly desirable sources include spectroscopy [13], biosensing [14], and quality inspection in various industries [15–17]. THz waves also have astronomical applications [1, 18].

In an experimental paper by Zanola *et al.* [3], the generation of tunable and narrow linewidth mm-wave signals is demonstrated utilising a semiconductor monolithic device. The device was based on the novel scheme of photomixing assisted by mutual injection locking through FWM. In the work of Zanola *et al.*, three single-mode distributed feedback (DFB) lasers were utilised.

This work will make a detailed study of the different behaviours of two lasers, utilising FWM mediated by injection locking in a third laser, paying particular attention to the different behaviours of the system observed within the different locking regions [1], but examining a broader range of parameter values than those considered experimentally by Zanola *et al.* [3], with a view to exploring and optimising the efficiency of the system while operating under the locked condition.

A potential field of application for the system described here is to shine the output from the scheme onto a photoconductive antenna [1, 8, 19] with the potential of generating a fixed frequency output. In a typical photoconductive photomixing scheme, two linearly polarised laser beams, whose difference in central frequencies fall within a defined frequency range, are applied to a DC biased photoconductor film, with the resulting difference frequency emitted by the antenna [19].

2 Background

2.1 Injection-locking

The system under consideration here utilises both injection locking and FWM. Over the past 25 years or so, the world of optics has demonstrated the durability and efficient approach that the injection locking scheme provides for improving the spectral and dynamic performance of directly modulated laser diodes [20–22]. Injection locking is achieved when the frequency and phase of an oscillator (slave oscillator) are locked through direct coupling from a second oscillator (master oscillator) [20]. The system in this study utilises two lasers, set-up similarly to a bidirectional configuration, utilising FWM mediated by injection locking in a third laser. In the system presented here, a fraction of the light from the first laser (depending on the value of injection rate, κ_c) is injected into the cavity of the second laser, as well as, at the same time, a fraction of light from the second laser (again, depending on the value of injection rate) is injected into the cavity of the first laser. However, as will be described, this injection process is mediated by a third laser diode that uses a FWM process to bring about a non-zero frequency difference between the two locked lasers [1].

2.2 Four-wave mixing

FWM may be described as the interaction of three separate electromagnetic fields in order to produce a fourth [23] through the third-order nonlinear susceptibility [24]. This produces many different frequency components, including the 'clone' signals defined below. The FWM scheme utilised in this study is based on the monolithic FWM scheme fabricated by Zanola *et al.* [3], where three separate, but monolithically integrated, semiconductor lasers were utilised in order to generate mm-wave signals which are both

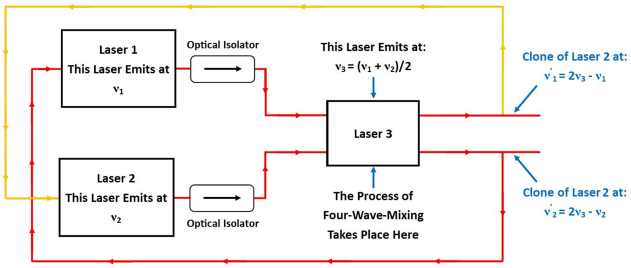

Fig. 1 *Laser configuration for the photomixing assisted by mutual injection locking and the FWM technique [1, 3]*

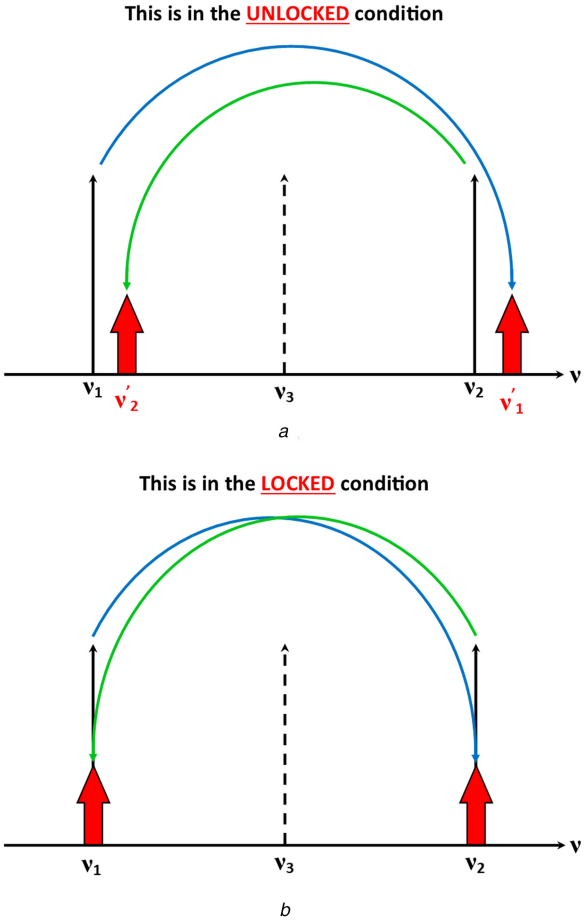

Fig. 2 *Lasers 1 and 2 operating*
(a) Under the unlocked condition, ***(b)*** Under the locked condition [1, 3]

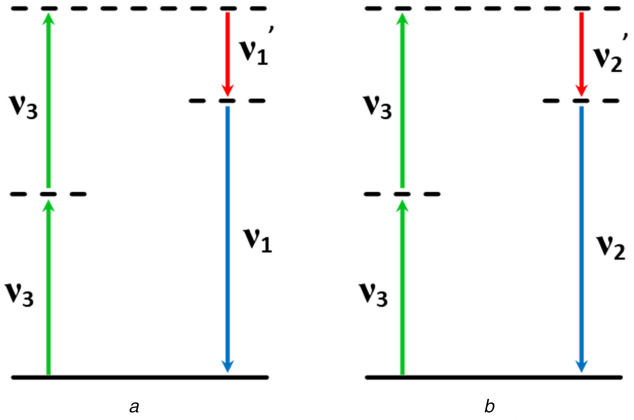

Fig. 3 *Energy-level descriptions of the two FWM processes taking place*
(a) Illustrating the generation of clone frequency ν'_1, ***(b)*** Illustrating the generation of clone frequency ν'_2 [1]

narrow and tunable. In the device demonstrated by Zanola *et al.*, two DFB lasers, with frequencies of ν_1 and ν_2, respectively, are injected into laser 3, emitting at the frequency of ν_3. Lasers 1 and 2 are subsequently locked through mutual injection, mediated by the process of FWM, which takes place within the third laser [3]. This is illustrated in Fig. 1. Through the FWM process, two new conjugate signals are generated (i.e. where the conjugated fields have a reversed propagation direction but retain their amplitudes and phases) that are 'clones' of the signals from lasers 1 and 2 [3]. The clone signals have the frequencies $\nu'_1 = 2\nu_3 - \nu_1$ and $\nu'_2 = 2\nu_3 - \nu_2$. The clone signal of laser 1, ν'_1, is then injected back into the cavity of laser 2, and the clone signal of laser 2, ν'_2, is injected back into the cavity of laser 1 [3]. If these clone signals' frequencies differ significantly from the frequencies ν_1 and ν_2 of lasers 1 and 2, then the two lasers will not be injection locked. This condition is depicted in Fig. 2*a*. In the special case where laser 3 is operating at the frequency $\nu_3 = (\nu_2 + \nu_1)/2$, the conjugate FWM signals will have the frequencies of $\nu'_1 = \nu_2$ and $\nu'_2 = \nu_1$ [3]. In order for the injection locking condition to be potentially realised, these conditions must be met, whereby the clone signals coincide with the original signals. Under these conditions, laser 1 will potentially be injection-locked to the clone signal from laser 2. At the same time, laser 2 will potentially be injection-locked to the clone signal from laser 1. When these conditions are met, injection locking is achieved with a non-zero frequency spacing between the frequencies of lasers 1 and 2, which are mutually coupled through their conjugate FWM signals. Under these conditions, the frequency separation, $\nu_2 - \nu_1$, would lie within the THz frequency range. This is illustrated in Fig. 2*b*. It is also worth noting that the lasers will not only lock when the clone signal frequencies coincide exactly with the original laser frequencies (i.e. when $\nu'_1 = \nu_2$ and $\nu'_2 = \nu_1$), but also if the clone signal frequencies are different but sufficiently close to the original frequencies of lasers 1 and 2. The upshot of all of this is that the beat signal that would be generated if the signals from lasers 1 and 2 were photomixed is a potentially pure radiofrequency signal [3, 25]. Zanola *et al.* demonstrated this scheme to be an innovative and compact structure to potentially generate spectrally pure signals within the THz gap [1, 3]. The work of Zanola *et al.* was only limited by the stopband gratings that were used in the DFBs, hence the only operation in the GHz range was achieved. They concluded that if gratings with larger stopbands were used, then wider tunability of the operating frequency could be achieved [3]. As the bandwidth of the FWM can exceed several THz [25–27], this indicates the feasibility of the system presented in this study for potentially producing THz radiation.

3 System model

This work studies the full range of behaviours of the system such as that implemented experimentally by Zanola *et al.* [3]. In the system examined here, it is possible to treat the interactions occurring inside the cavity of the third laser as two, separate, FWM processes [1]; one where the output from laser 1, at frequency ν_1, interacts with the output from laser 3, at frequency ν_3, in order to generate a conjugate signal at $\nu'_1 = 2\nu_3 - \nu_1$, and the second where the output from laser 2, at frequency ν_2, interacts with the output from laser 3, at frequency ν_3, in order to generate a conjugate signal at $\nu'_2 = 2\nu_3 - \nu_2$. Two energy-level diagrams [28, 29] may be used to describe these processes, as illustrated in Figs. 3*a* and *b* [1].

The FWM system under consideration here may also be represented mathematically [1]. The nonlinear polarisation may be defined as [28]

$$\tilde{P}^3(t) = \epsilon_0 \chi^{(3)} \tilde{E}^3(t), \tag{1}$$

where $\tilde{P}(t)$ is defined as the nonlinear part of the electric polarisation of the material, ϵ_0 is the permittivity of free space, $\chi^{(3)}$ is the third-order nonlinear optical susceptibility, and $\tilde{E}(t)$ is the applied optical field strength.

The FWM system under consideration here consists of three frequency components, and as such, the polarisation from (1) may

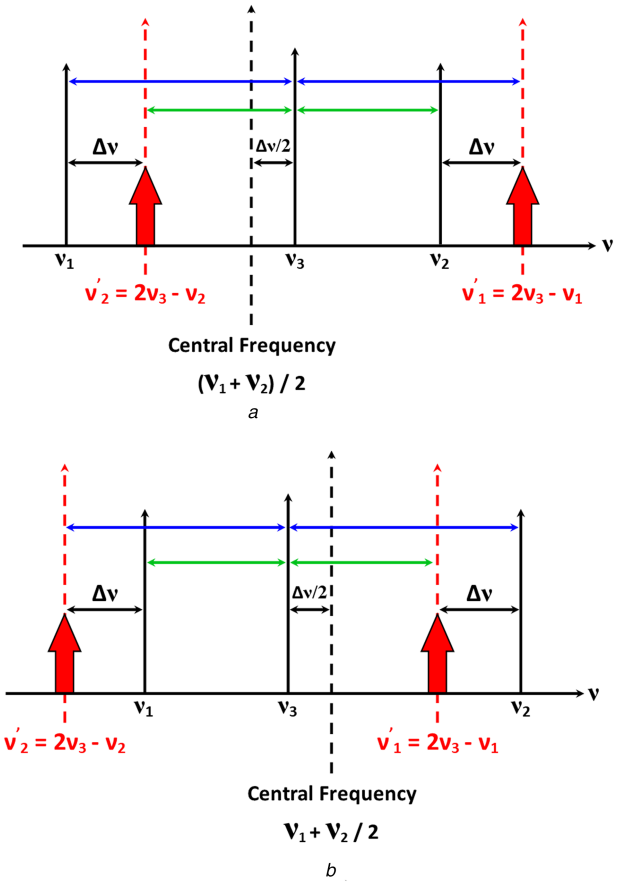

Fig. 4 *Illustration of the detuning frequency, Δv, as a function of the deviation of the clone signals from v_1 and v_2*

(a) Illustration of detuning frequency, $\Delta\nu$, as a function of the deviation of the clone signals from ν_1 and ν_2 for positive detuning [1], ***(b)*** Illustration of detuning frequency, $\Delta\nu$, as a function of the deviation of the clone signals from ν_1 and ν_2 for negative detuning [1]

Table 1 Laser parameters used in the investigation [32, 33]

Parameter	Symbol	Value
linewidth enhancement factor	α	5
carrier lifetime	τ_n	2 ns
photon lifetime	τ_p	2 ps
gain coefficient	g	$15 \times 10^3\ \mathrm{s}^{-1}$
gain saturation coefficient	ϵ	1.5×10^{-17}
carrier number at transparency	N_0	1.5×10^8

be induced by an applied field also consisting of three frequency components [28]

$$\tilde{E}(t) = E_1 \mathrm{e}^{-\mathrm{i}(2\pi\nu_1)t} + E_2 \mathrm{e}^{-\mathrm{i}(2\pi\nu_2)t} + E_3 \mathrm{e}^{-\mathrm{i}(2\pi\nu_3)t} + c \cdot c\,. \tag{2}$$

The resulting expression $\tilde{E}^3(t)$ contains 44 different frequency components if the positive and negative frequencies are distinct. These frequencies are defined as [28] (and the negative of each)

$$\begin{aligned} &\nu_1, \nu_2, \nu_3, 3\nu_1, 3\nu_2, 3\nu_3, (\nu_1 + \nu_2 + \nu_3), (\nu_1 + \nu_2 - \nu_3), \\ &(\nu_1 + \nu_3 - \nu_2), (\nu_1 + \nu_3 - \nu_1), (\nu_2 + \nu_3 - \nu_1), (2\nu_1 \pm \nu_2), \\ &(2\nu_1 \pm \nu_3), (2\nu_2 \pm \nu_1), (2\nu_2 \pm \nu_3), (2\nu_3 \pm \nu_1), (2\nu_3 \pm \nu_2)\,. \end{aligned} \tag{3}$$

For the work under consideration here, phase conjugate injection [30, 31] is going to be considered (which is defined in more detail in the Appendix). This is used to model a similar system to that implemented experimentally by Zanola *et al.* [3], specifically creating the frequency components of $2\nu_3 - \nu_1$ and $2\nu_3 - \nu_2$, as these are the only ones similar in frequency to ν_1 and ν_2 [1].

The laser rate equations presented in the work of Peters-Flynn *et al.* [32, 33] will be the foundation for the three-laser FWM model presented in this study. These rate equations are related to those initially developed by Lang and Kobayashi [34], however, for the work presented here, the rate equations have been modified to accommodate optical phase conjugate injection [1].

The rate equations representing the system are represented by (4)–(7), where $\overline{A_{1,2}(t)}$ represents the phase-conjugated fields, and $\Delta\omega = 2\pi\Delta\nu$ represents the circular detuning frequency. It is emphasised here that the quantity $\Delta\nu$ is not in the THz range frequency separation, but rather the detuning frequency between the original signals and the clones, as illustrated in Fig. 4. This is different from the frequency difference $(\nu_2 - \nu_1)$, which is of course in the THz frequency range. Equation (7) represents the gain in the medium and is applied to both the first and second lasers, respectively. The model is simulated using the parameter values defined in Table 1 [32, 33]. Here, it is emphasised that the time of flight between the coupled electric fields in the model is assumed to be zero [1]

$$\frac{\mathrm{d}A_1(t)}{\mathrm{d}t} = \frac{1}{2}(1 + \mathrm{i}\alpha)\left[G_1 - \frac{1}{\tau_p}\right]A_1(t) + \kappa_c \overline{A_2(t)}\,\mathrm{e}^{\mathrm{i}\Delta\omega t}, \tag{4}$$

$$\frac{\mathrm{d}A_2(t)}{\mathrm{d}t} = \frac{1}{2}(1 + \mathrm{i}\alpha)\left[G_2 - \frac{1}{\tau_p}\right]A_2(t) + \kappa_c \overline{A_1(t)}\,\mathrm{e}^{\mathrm{i}\Delta\omega t}, \tag{5}$$

$$\frac{\mathrm{d}N_{1,2}(t)}{\mathrm{d}t} = \frac{J}{e} - \frac{N_{1,2}(t)}{\tau_n} - G_{1,2}\left|A_{1,2}(t)\right|^2, \tag{6}$$

$$G_{1,2} = \frac{g(N_{1,2}(t) - N_0)}{1 + \epsilon\left|A_{1,2}(t)\right|^2}\,. \tag{7}$$

Two equations are defined for each of the two lasers; one represents the slowly varying complex electric field amplitude, $A_{1,2}(t)$, in the laser cavity for the first laser or the second laser, respectively, defined by (4) and (5), and the other represents the number of charge carriers, $N_{1,2}(t)$, in the gain medium for the first laser or the second laser, respectively, defined by (6). As discussed in the introduction, light from laser 1 is injected into the cavity of laser 2, and likewise, light from laser 2 is injected into the cavity of laser 1. As such, the system employed here is similar to a bidirectional injection-locked scheme. As this system implements injection-locking mediated by FWM, to correctly implement the FWM process, both electric fields must be conjugated. This is done in order to simulate the effect of generating the two clone signals from lasers 1 and 2, which are two new conjugate FWM signals. These conjugated signals are then multiplied by the injection rate, κ_c, together with the frequency detuning terms, $\Delta\nu$. It is worth noting here that both the frequency detuning terms from (4) and (5) are positive; this is because the frequency detuning, $\Delta\nu$, in this work defines the deviation of the clone signals ν_1' and ν_2' from ν_2 and ν_1, respectively (not the deviation of the third laser from its centre frequency), as depicted in Figs. 4*a* and *b*. For positive values of frequency detuning, ν_1' and ν_2' will move positively with respect to ν_2 and ν_1, as illustrated in Fig. 4*a*. As a result, there will be an equal frequency spacing between $\nu_1 \to \nu_3$ and $\nu_3 \to \nu_1'$, and also between $\nu_2' \to \nu_3$ and $\nu_3 \to \nu_2$. For negative detuning, the clone signals will move negatively with respect to ν_1 and ν_2, as illustrated in Fig. 4*b*, and as a result, there will be equal frequency spacing between $\nu_2' \to \nu_3$ and $\nu_3 \to \nu_2$, and also between $\nu_1 \to \nu_3$ and $\nu_3 \to \nu_1'$. It should be noted that the deviation of the clone signals from ν_1 and ν_2 will be twice that of the deviation of ν_3 from its central frequency, as shown in (8) [1]:

$$\begin{aligned} \Delta\nu = \nu'_2 - \nu_1 &= 2\nu_3 - \nu_1 - \nu_1 = 2(\nu_3 - \nu_1), \\ \therefore \nu_3 - \nu_1 &= \frac{\Delta\nu}{2}\,. \end{aligned} \tag{8}$$

The deviation of laser 3 from its central frequency value is of course what causes the system to either operate under the locked or unlocked condition. However, for the work presented in this study,

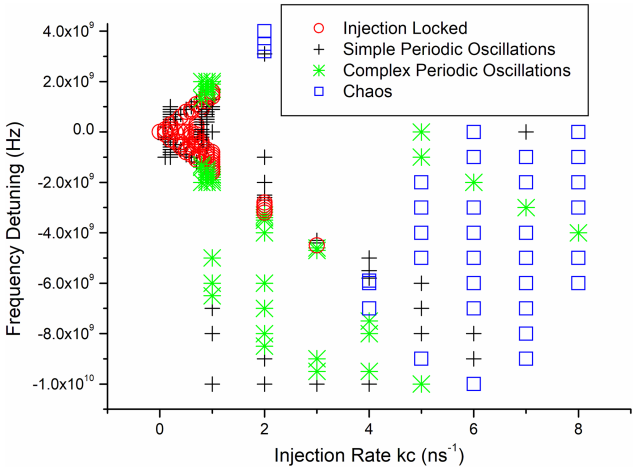

Fig. 5 *System behaviour for bidirectional phase conjugate injection, for injection rates, κ_c, ranging from 0.1 to 8.0 ns^{-1}, for detuning frequencies, $\Delta\nu$, extending from −10 to 4 GHz [1]*

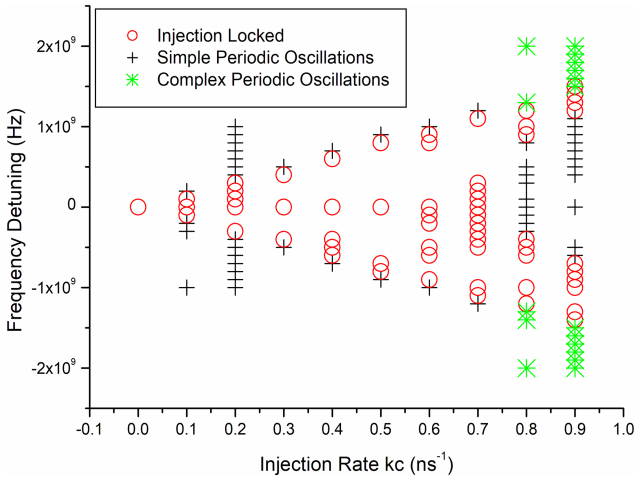

Fig. 6 *System behaviour for bidirectional phase conjugate injection, for injection rates, κ_c, ranging from 0.1 to 0.9 ns^{-1}, for detuning frequencies, $\Delta\nu$, extending from −2 to 2 GHz [1]*

it is the deviations of ν_1' and ν_2' from ν_2 and ν_1 that have been modelled. Thus, it is this quantity that will be referred to as the detuning frequency, $\Delta\nu$ [1]. It is again emphasised that this is not the THz range frequency separation.

4 FWM model: locking region analysis

For the work presented in this study, the system was simulated with the injection rate, κ_c, values ranging from 0.1 to 8.0 ns^{-1}, with frequency detuning values, $\Delta\nu$, extending from −10 to 4 GHz. This is depicted in Fig. 5, where the black crosses resemble cases where the lasers' carrier and photon number output are oscillating periodically, the green stars resemble a periodic, yet more complex waveform containing multiple frequencies, and the blue squares resemble regions where the lasers' carrier and photon number exhibit a chaotic behaviour, with multiple, unrelated frequencies apparent in the system. The locking condition between the two lasers is the final region, and these are represented by red circles. This is where continuous wave (CW) operation is observed [1].

Details from Fig. 5 are shown in Fig. 6, where Fig. 6 shows the locking region with injection rate values ranging from 0.1 and 0.9 ns^{-1} for detuning frequency values extending from −2 to 2 GHz. Figs. 5 and 6 show the range of different behaviours exhibited by the system. For injection rates extending from 0.1 to 0.7 ns^{-1}, the system shows behaviours expected from a typical bidirectional injection locked system, whereby the locking region shows a symmetrical tendency for both positive and negative frequency

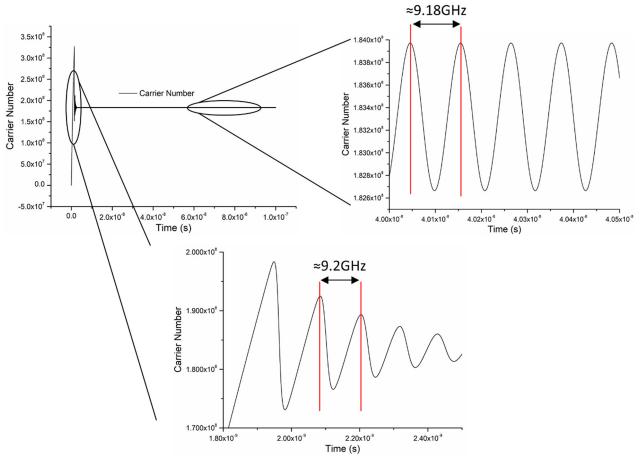

Fig. 7 *Carrier number output with an injection rate, κ_c, of 0.8 ns^{-1} with a frequency detuning, $\Delta\nu$, of 0 GHz with periodic oscillations with a frequency of ≃9.18 GHz [1]*

detuning values. Here, both lasers lock for each value of detuning frequency considered. When the injection rate of the system is increased between 0.8 and 1.0 ns^{-1}, the system still displays similarities to those of a bidirectional injection locked system, however, the system only locks for larger values of positive and negative frequency detuning (for 0 or small frequency detuning, the system simply oscillates at ∼9.2 GHz); taking an injection rate of 0.9 ns^{-1} as an example, between detuning frequencies of −700 MHz and −1.4 GHz, and between 1.2 and 1.4 GHz, the two lasers lock, as per the red circles. In between these two regions, the system simply oscillates continuously at ∼9.2 GHz (shown as black crosses), corresponding to the relaxation oscillation frequency of the system, as discussed later. It is also noted that the stronger the injection rate, the narrower the locking region for positive detuning values, hence indicating that the linewidth enhancement factor, α, in both lasers is having an increased effect on the system, thus making locking more difficult with positive frequency detuning values. When outside the locking region, the system oscillates periodically, with multiple frequencies present in the system, shown as green stars. As the injection rate is extended from 0.1 to 0.7 ns^{-1}, it is interesting to note that the width of the locking region increases [1].

4.1 Simple periodic oscillations

4.1.1 Relaxation oscillations: In this section, the region of black crosses is considered, where the system simply oscillates approximately sinusoidally, as can be seen in Fig. 7. When this behaviour is apparent, regardless of the frequency detuning value, the system simply oscillates with a frequency of ∼9.2 GHz each time. By analysing the frequency of the relaxation oscillations of the laser rate equations for the parameter values in Table 1, a frequency value of ∼9.0–9.2 GHz is found. This is similar in value to those obtained for the complete system's oscillations. This indicates that the frequency of these oscillations is related to the laser relaxation oscillation frequency. It is also apparent from Fig. 7 that these oscillations are undamped oscillations. Increasing the injection current causes the frequency of these oscillations also to increase, offering further evidence that the frequency of these oscillations is related to the relaxation oscillations frequency of the system. In these regions, the lasers are not injection-locked (as a non-CW behaviour is observed), but the carriers and photons in both lasers exhibit the same time domain pattern [1].

It should be noted that this behaviour is only observed for injection rates of 0.8 ns^{-1} or above, when the system will only lock for larger values of positive and negative detuning (as discussed previously), and when the system starts to become asymmetrical in behaviour, which leads to the generalised locking region, which will be discussed in more detail in Section 5. The black crosses for injection rates above 0.8 ns^{-1} in Figs. 5 and 6 represent this region of behaviour.

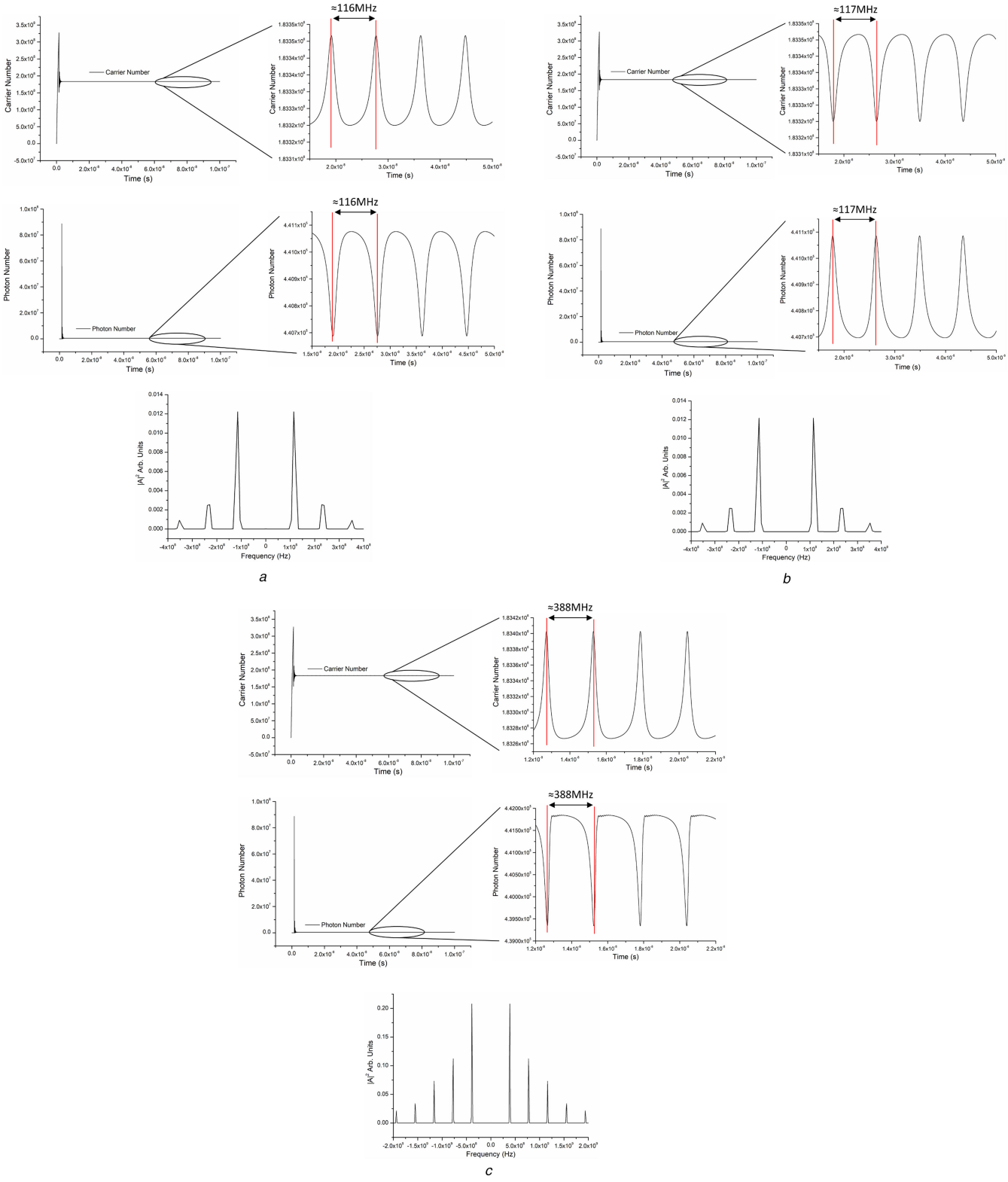

Fig. 8 *Typical behaviour observed for single periodic oscillations*

(a) Carrier (top panel), photon (middle panel) and FFT (bottom panel) outputs with $\kappa_c = 0.1\,\text{ns}^{-1}$ and $\Delta\nu = -200\,\text{MHz}$ [1], ***(b)*** Carrier (top panel), photon (middle panel) and FFT (bottom panel) outputs with $\kappa_c = 0.1\,\text{ns}^{-1}$ and $\Delta\nu = +200\,\text{MHz}$ [1], ***(c)*** Carrier (top panel), photon (middle panel) and FFT (bottom panel) outputs with $\kappa_c = 0.5\,\text{ns}^{-1}$ and $\Delta\nu = -900\,\text{MHz}$ [1]

When the system is operating with lower injection rates, extending from 0.1 to 0.7 ns^{-1}, the oscillations of ∼9.2 GHz are not observed. This region is, of course, the region where strong symmetrical locking behaviour is apparent, and behaviours typical of Figs. 8*a*–*c* are observed [1].

4.1.2 Single periodic oscillations: Figs. 8*a*–*c* show the typical oscillations observed when a black cross is apparent in Figs. 5 and 6, where the injection rate is extended from 0.1 to 0.7 ns^{-1}. Figs. 8*a* and *b* show the response of the system for an injection rate of 0.1 ns^{-1} for detuning frequencies of −200 and +200 MHz, respectively, and Fig. 8*c* shows the response of the system for an injection rate of 0.5 ns^{-1} for a detuning frequency of −900 MHz. In all figures, a clear periodic pattern is apparent in the time domain trace of the carriers and photons, which all appear to display a strong fundamental frequency, where frequencies between 116

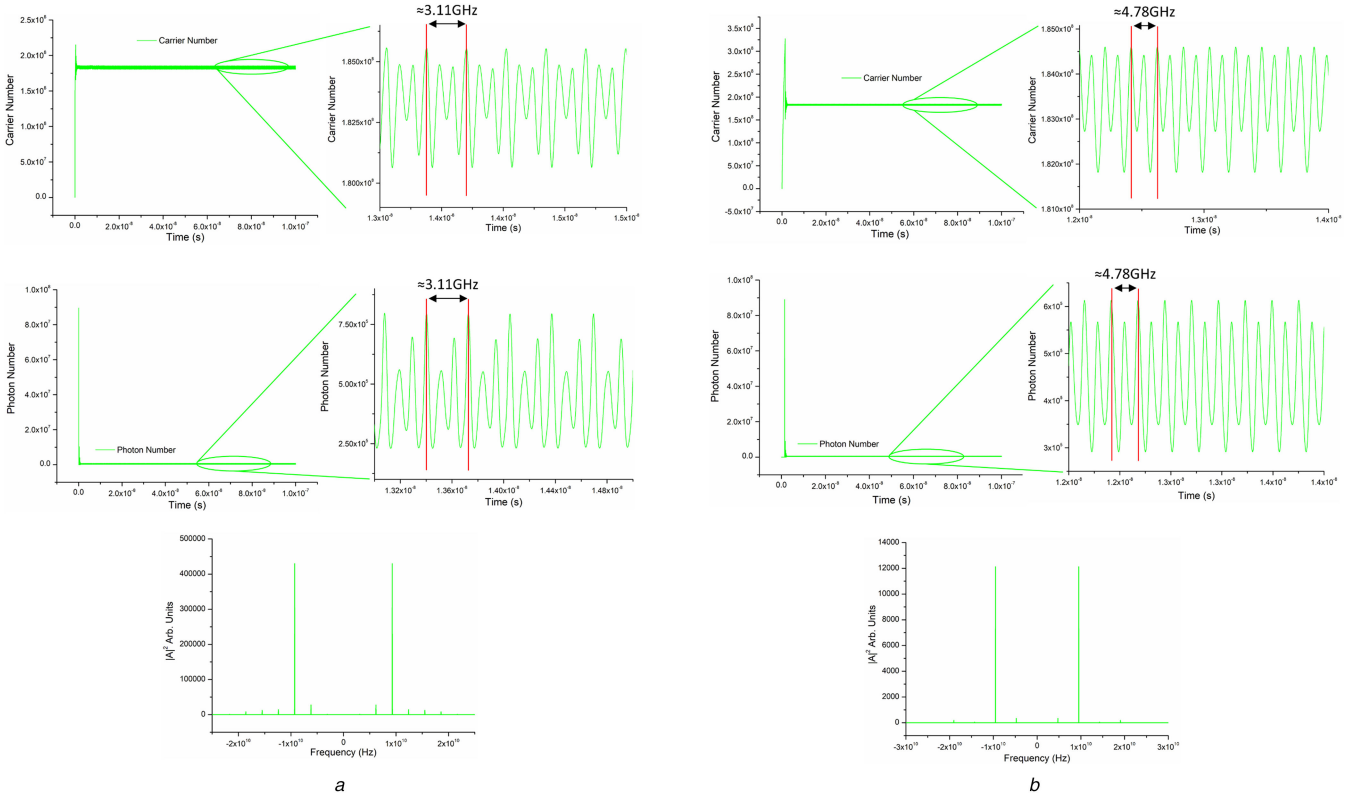

Fig. 9 *Typical behaviour observed for complex periodic oscillations*

(a) Carrier (top panel), photon (middle panel) and FFT (bottom panel) outputs with $\kappa_c = 5.0\,\text{ns}^{-1}$ and $\Delta\nu = 0\,\text{Hz}$ [1], ***(b)*** Carrier (top panel), photon (middle panel) and FFT (bottom panel) outputs with $\kappa_c = 3.0\,\text{ns}^{-1}$ and $\Delta\nu = -4.6\,\text{GHz}$ [1]

MHz (Fig. 8*a*) and 388 MHz (Fig. 8*c*) are observed. In this region, the lasers are again not injection-locked, but exhibit the same time domain pattern in the carriers and photons in both lasers [1].

To confirm the dominance of the fundamental frequency under these conditions, the spectrum of the photon number for each case is plotted, estimated using a fast-Fourier-transform (FFT) using a Hamming window, with the DC component removed for clarity. There is a clear harmonic relationship between the frequencies present in the system, with the fundamental frequency in each case exhibiting the highest power (∼116 MHz in Fig. 8*a*, and ∼388 MHz in Fig. 8*c*). The other frequency components within the spectrum are harmonically related to the fundamental frequency [1]. In the FFT of Fig. 8*a*, additional peaks are observed at 232 and 348 MHz, and in the FFT of Fig. 8*c*, additional peaks are observed at 776 MHz, 1.164 GHz etc., thus confirming the harmonic relationship between the fundamental frequency and other frequency components.

Figs. 8*a–c* demonstrate behaviours typical of those observed when the system was operating with injection rate values ranging from 0.1 to 2 ns^{-1} when the system was operating outside of the locking region only. When operating outside of this range, contrasting behaviours were observed, which will be described and analysed later [1].

4.2 Complex periodic oscillations

In this section, the region of green stars in Figs. 5 and 6 is considered. Examples of the observed time-domain behaviours are given in Figs. 9*a* and *b*, which show the behaviours for an injection rate of 5.0 ns^{-1} with a detuning frequency of 0 Hz, and an injection rate of 3.0 ns^{-1} with a detuning frequency of −4.6 GHz. This regime of behaviour shows a periodic response once more, however, a more complex waveform is observed, indicating the presence of multiple frequency components. For an injection rate of 5.0 ns^{-1} and detuning frequency of 0 Hz (Fig. 9*a*), the fundamental frequency component was measured to be 3.11 GHz, whereas for an injection rate of 3.0 ns^{-1} and detuning frequency of −4.6 GHz (Fig. 9*b*), the fundamental frequency component was measured to be 4.78 GHz [1].

As with the periodic oscillations, to elucidate these multiple frequencies, FFTs of the photon number outputs have been plotted. These are displayed in the lowest plots of Figs. 9*a* and *b*, where the DC components have once more been removed for clarity. In these figures, there is again a harmonic relationship between the frequencies present in the system, however, in these cases, the fundamental frequency does not have the highest power. In the case of Fig. 9*a*, the frequency with the highest power appears to be the third harmonic (∼9.33 GHz), whereas, in the case of Fig. 9*b*, the second harmonic appears to contain the highest power (∼9.56 GHz). The other frequency components present in the spectra of both figures are harmonically related to the fundamental frequency [1].

When a green cross is displayed in Figs. 5 and 6, behaviours comparable to those shown in either Fig. 9*a* or Fig. 9*b* are apparent. In these regions, the lasers are again not injection-locked, but follow the same time domain pattern as the carriers and photons in both lasers [1].

4.3 Chaos

The blue crosses from Figs. 5 and 6 represent a chaotic behaviour in the system. The regions of chaotic behaviour only become apparent when the system is operating with an injection rate of at least 2.0 ns^{-1} and a detuning frequency value of −4 GHz when the behaviour of the system has become more complex. Fig. 10 demonstrates an example of the typical chaotic behaviour observed. As can be seen in Fig. 10, there are clearly multiple, non-harmonically-related frequencies apparent in the system, and these multiple frequencies appear to include a frequency component of ∼9.2 GHz. It is again interesting to note that the frequency component observed from the chaos in Fig. 10 is approximately equal to the relaxation oscillation frequency, as discussed previously. As CW operation is desired from this system, a chaotic response, such as that seen in Fig. 10, should be avoided for the applications under consideration here. As the injection rate is increased, the regions of chaotic behaviour become more apparent;

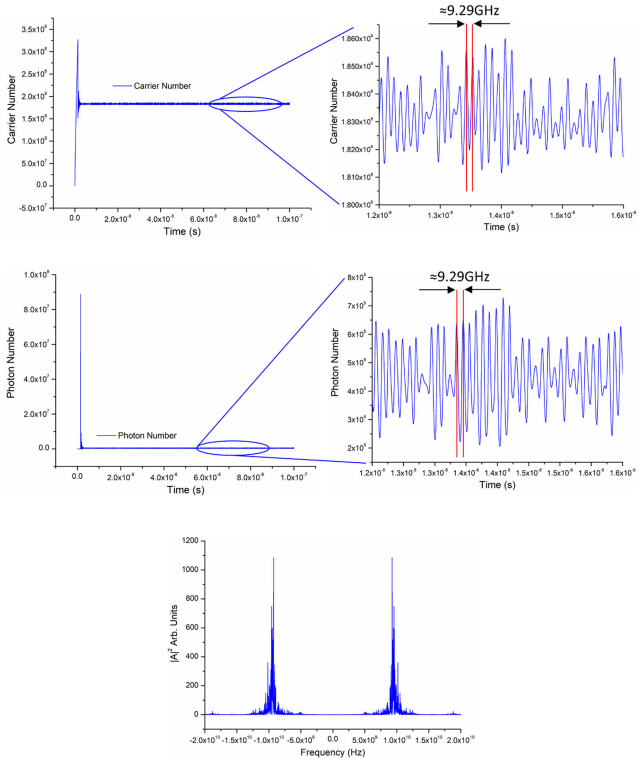

Fig. 10 *Carrier (top panel), photon (middle panel) and FFT (bottom panel) outputs with* $\kappa_c = 5.0\,ns^{-1}$ *and* $\Delta\nu = -4\,GHz$ *[1]*

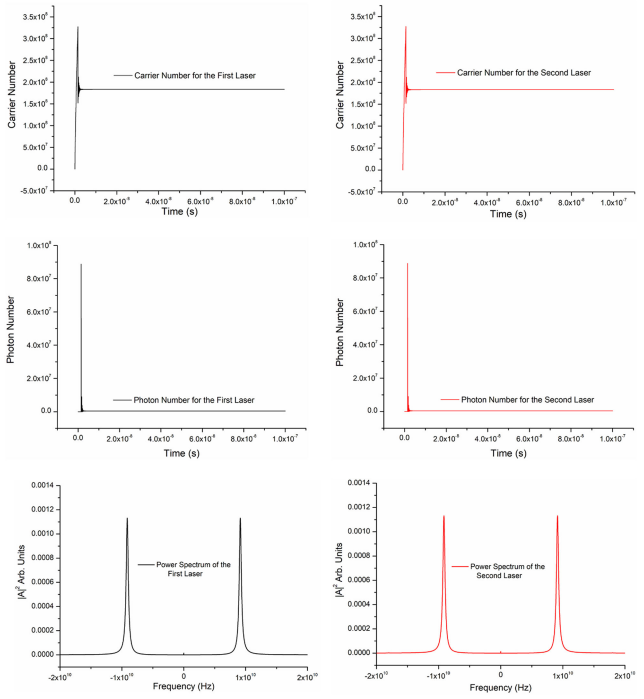

Fig. 11 *Carrier (top panel), photon (middle panel) and FFT (bottom panel) outputs with* $\kappa_c = 0.6\,ns^{-1}$ *and* $\Delta\nu = -500\,MHz$ *[1]*

at an injection rate of 5.0 ns^{-1}, the region of chaotic behaviour has a width of 4 GHz, whereas the region of chaotic behaviour has a width of 6 GHz for an injection rate of 7.0 ns^{-1} [1].

As was the case for the periodic and multiple periodic responses, the spectra of the photon number signals are plotted using FFTs in order to corroborate whether the carriers and photons are actually exhibiting chaotic behaviour [1]. Again, the DC component has been removed for clarity. The FFT is shown in the lower plot of Fig. 10, and it is clear that it is difficult to distinguish the individual peaks in the spectrum, indicating a clear chaotic behaviour being exhibited by the system in these regions [1].

4.4 Injection-locked

The red circles depicted in Figs. 5 and 6 indicate regions of locking between the first and second lasers, and this is the final area of interest for this work. The time domain representation of the locking is illustrated in Fig. 11, where the carriers are represented in the top figure, the photons are represented in the middle figure, and the FFT is represented in the bottom figure. Fig. 11 presents the locking condition for an injection rate of 0.6 ns^{-1} and a detuning frequency of −500 MHz. When the system locks, a clear CW operation is observed, where there is a clear absence of any oscillations in the carrier and photon output responses. In this case, the steady-state value of the carriers and photons output responses have settled to very similar values in both lasers. It is this condition that gives a fixed frequency separation between the two lasers [1].

The FFT plots for both lasers shows that only a single frequency is present for both lasers while the system is operating within the locked condition [1].

Considering the locking behaviour for different injection rates, it has been seen that increasing the injection rate causes the system to take more time to lock, where the transient oscillations take more time to diminish than with lower injection rates. This is to be expected as increasing κ_c increases the amplitude of the sinusoidal oscillations, and as such the oscillations in the system take longer to decay to a negligible level.

Also, it can be noted that as the frequency detuning is increased, the system takes less time to lock than with lower frequency detuning values; e.g. at an injection rate of 0.9 ns^{-1}, the system takes longer time to lock with a frequency detuning of −700 MHz than it does with a frequency detuning of −1.4 GHz. This is also true for positive frequency detuning values. For negative values of detuning, the system very rapidly locks on the border of the locking region. When the system operates with an injection rate of 0.9 ns^{-1} and a frequency detuning of −1.4 GHz, the system will lock and operate in CW the instant after the turn-on transient of the system, before losing synchronisation at a frequency detuning of −1.5 GHz. For positive values of detuning, this is not the case (for injection rates >0.8 ns^{-1}). For the generation of a stable frequency difference between the two lasers, the regions denoted by red circles will be more useful as these regions will give the best spectral purity, which will lead to a narrower linewidth.

5 Locking condition analysis

To establish what kind of behaviour the system exhibits while operating within the locking regions, an analysis on the optical phase, φ, and its rate of change $d\varphi/dt$ is done. This is done in order to analyse the instantaneous frequency of the two lasers. After the turn on transient of the laser, φ varies linearly with time, thus indicating a constant frequency offset from the free-running frequency of the laser. When operating under the locked condition, there is no superimposed modulation in the response of φ or $d\varphi/dt$. When operating outside of the locking region, superimposed modulation is observed in φ and $d\varphi/dt$, thus indicating a phase and frequency modulation of the signals; the deviation in $d\varphi/dt$ follows the same pattern as the deviation in photon number (the time domain trace) [1].

Fig. 12*a* shows the mean value of the frequency offset, $d\varphi/dt$, as a function of detuning frequency when the system was operating with an injection rate of 0.2 ns^{-1}, with the red circles and black crosses corresponding to the locking condition and periodic condition, respectively, between the lasers, as per Figs. 5 and 6. It is clear from the figure that there is a linear relationship between the frequency offset and the detuning frequency while operating within the locking region, and there is a clear transition in behaviour either side of the locking region, where the frequency offset shows a different, nonlinear dependence on detuning. The figure also clearly shows that the lasers lock at each point of detuning frequency within the linear region [1].

Fig. 12*b* shows the mean value of the frequency offset against detuning frequency when the system operates with an injection rate of 0.9 ns^{-1}. Here, it is clear to see again the linear relationship between the frequency offset and detuning when the laser is

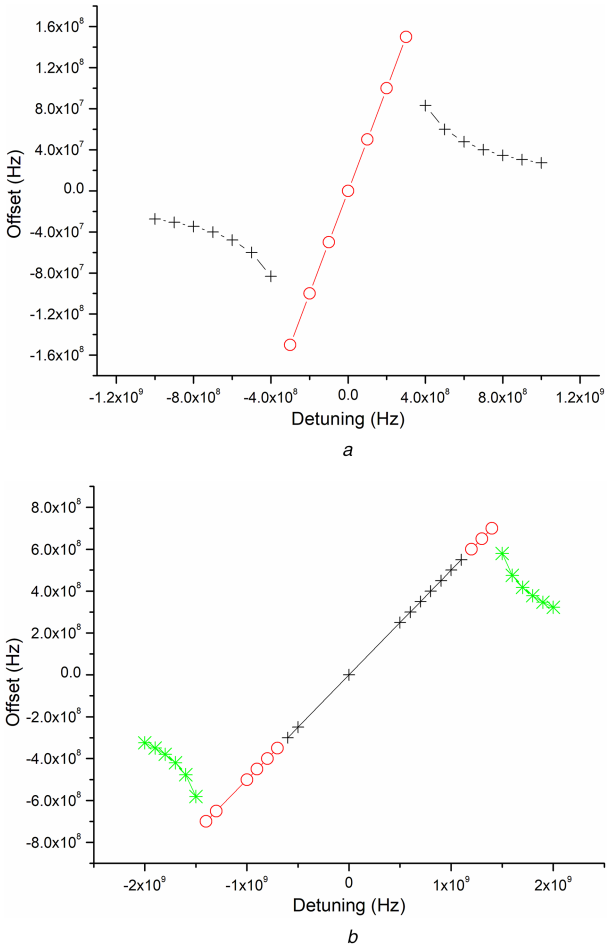

Fig. 12 *Mean value of the frequency offset, dφ/dt, as a function of the detuning frequency*

(a) Analysis of the frequency offset against detuning frequency for $\kappa_c = 0.2\,\mathrm{ns}^{-1}$ [1], ***(b)*** Analysis of the frequency offset against detuning frequency for $\kappa_c = 0.9\,\mathrm{ns}^{-1}$ [1]

operating within the generalised locking region, as was seen with an injection rate of $0.2\ \mathrm{ns}^{-1}$. However, it is interesting to note, as per Fig. 6, the system only locks between −1.4 GHz and −700 MHz, and between +1.2 and +1.5 GHz, at either end of the generalised locking region, with a periodic response observed in the central region (as discussed previously), hence, this is why this region is called the generalised locking region. This is due to the linewidth enhancement factor, α, in both of the lasers having an increased effect on the system, thus causing fewer locking conditions with positive detuning. As the injection rate is increased, this eventually causes the system to become asymmetrical in behaviour. Again, outside of the generalised locking region, the frequency offset shows nonlinear dependence on detuning, where $\mathrm{d}\varphi/\mathrm{d}t$ is not constant, but oscillates around a constant value following the same pattern as the green stars (as discussed previously) [1].

6 Conclusion

This study introduced numerical studies of a three-laser FWM scheme, which employed injection locking to maintain a locking condition with a non-zero separation of the lasers' frequency, in order to potentially realise THz radiation while operating under the locked condition.

Through the analysis, four distinct regions of behaviour were observed in the response of the system. The first area was where the carriers and photons oscillated periodically in an approximately sinusoidal fashion, where these oscillations had a frequency approximately equal to the relaxation oscillation frequency, thus suggesting a simple relationship between these oscillations and the relaxation oscillation of the laser diodes. Increasing the injection current caused an increase in this frequency. This region of periodicity also exhibited a harmonic relationship between the fundamental frequency and the other frequency components present in the FFT spectrum, with the fundamental frequency component containing the highest power.

The second region was where multiple frequencies were present in the response of the system, again with a harmonic relationship between the fundamental frequency and other frequency components, however, in this case, the fundamental frequency did not contain the highest power.

The third regime of behaviour was where the system exhibited a chaotic behaviour, and where the apparent frequency components were not harmonically related.

The locked condition was the final regime of behaviour observed in the system, where the two lasers' carriers and photons settled to a constant steady-state value after the relaxation oscillations and were operating in CW. For the best spectral purity, it is best for the system to operate under the locked condition, where a narrower linewidth will be observed because of the phase-locking between the lasers.

There was a clear linear relationship between the frequency offset and detuning frequency while operating in the locking region, and there was a clear transition in behaviour either side of the locking region, where the system showed a nonlinear relationship. It was found that for higher injection rates, although locking was only observed at either end of the generalised locking region, a clear linear relationship was still observed between the frequency offset and detuning frequency while operating in this generalised locking region.

Further work will profitably examine the response of the coupled laser system to introduced perturbations, and whether or not the three laser FWM scheme, operated in the locking region, provides a performance enhancement over the case of two uncoupled lasers, with a view of exploring the potential application advantage of operating within the generalised locking region.

7 References

[1] Roberts, D.: 'Semiconductor devices for generating terahertz radiation'. PhD thesis, School of Electronic Engineering, Bangor University, Bangor, UK, 2016

[2] Wang, Z., Liu, H., Huang, N., *et al.*: 'Efficient terahertz-wave generation via four-wave mixing in silicon membrane waveguides', *Opt. Express*, 2012, **20**, (8), pp. 8920–8929

[3] Zanola, M., Strain, M.J., Giuliani, G., *et al.*: 'Monolithically integrated DFB lasers for tunable and narrow linewidth millimetre-wave generation', *IEEE J. Quantum Electron.*, 2013, **19**, (4), doi: 10.1109/JSTQE.2012.2235412

[4] Sun, H., Ding, Y.J., Zotova, I.B.: 'THz spectroscopy by frequency-tuning monochromatic THz source: from single species to gas mixtures', *IEEE Sensors J.*, 2010, **10**, (3), pp. 621–629

[5] Mittleman, D., Jacobsen, R., Neelamani, R., *et al.*: 'Gas sensing using terahertz time-domain spectroscopy', *Appl. Phys. B, Lasers Opt.*, 1998, **67**, pp. 379–390

[6] Wang, S., Ferguson, B., Abbott, D., *et al.*: 'T-ray imaging and tomography', *J. Biol. Phys.*, 2003, **29**, (2–3), pp. 247–256

[7] Baker, C., Lo, T., Tribe, W.R., *et al.*: 'Detection of concealed explosives at a distance using THz technology', *Proc. IEEE*, 2007, **95**, (8), pp. 1559–1565

[8] Saeedkia, D., Mansour, R.R., Safavi-Naeini, S.: 'Analysis and design of a continuous-wave terahertz photoconductive photomixer array source', *IEEE Trans. Antennas Propag.*, 2005, **53**, (12), pp. 4044–4050

[9] Fitzgerald, A.J., Cole, B.E., Taday, P.F.: 'Nondestructive analysis of tablet coating thickness using terahertz pulsed imaging', *J. Pharm. Sci.*, 2005, **94**, (1), pp. 177–183

[10] Siegel, P.H.: 'Terahertz technology in biology and medicine', *IEEE Trans. Microw. Theory Tech.*, 2004, **52**, (10), pp. 2438–2447

[11] Scheller, M., Yarborough, J.M., Moloney, J.V., *et al.*: 'Room temperature continuous wave milliwatt terahertz source', *Opt. Express*, 2010, **18**, (26), pp. 27112–27117

[12] Siegel, P.H.: 'Introduction to terahertz (THz): technology and applications'. IEEE MTT-S Webinars, California Institute of Technology and THz Global, Pasadena, CA, USA, Presented on 12 January 2016

[13] Grinschkowsky, D., Keiding, S., Exter, M., *et al.*: 'Far-infrared time-domain spectroscopy with terahertz beams of dielectrics and semiconductors', *J. Opt. Soc. Am. B*, 1990, **7**, (10), pp. 2006–2015

[14] Debus, C., Bolivar, P.H.: 'Frequency selective surfaces for high sensitivity terahertz sensing', *Appl. Phys. Lett.*, 2007, **91**, (18), pp. 184102-1–184102-3

[15] Yasui, T., Yasuda, T., Sawanaka, K., *et al.*: 'Terahertz paintmeter for noncontact monitoring of thickness and drying progress in paint film', *Appl. Opt.*, 2005, **44**, (32), pp. 6849–6856

[16] Stoik, C.D., Bohn, M.J., Blackshire, J.L.: 'Nondestructive evaluation of aircraft composites using transmissive terahertz time domain spectroscopy', *Opt. Express*, 2008, **16**, (21), pp. 17039–17051

[17] Jördens, C., Koch, M.: 'Detection of foreign bodies in chocolate with pulsed terahertz spectroscopy', *Opt. Eng.*, 2008, **47**, (3), pp. 037003-1–037003-5
[18] Siegel, P.H.: 'THz instruments for space', *IEEE Trans. Antennas Propag.*, 2007, **55**, (11), pp. 2957–2965
[19] Saeedkia, D., Mansour, R.R., Safavi-Naeini, S.: 'The interaction of laser and photoconductor in a continuous-wave terahertz photomixer', *IEEE J. Quantum Electron.*, 2005, **41**, (9), pp. 1188–1196
[20] Zhao, X.: 'Optical injection locking on vertical-cavity surface-emitting lasers (VCSELs): physics and applications'. PhD thesis, Department of Electrical Engineering and Computer Science, California University, Berkeley, USA, 2008
[21] Parekh, D., Zhao, X., Hofmann, W., *et al.*: 'Greatly enhanced modulation response of injection-locked multimode VCSELs', *Opt. Express*, 2008, **16**, (26), pp. 21582–21586
[22] Chrostowski, L., Zhao, X., Chang-Hasnain, C.J.: 'Microwave performance of optically injection-locked VCSELs', *IEEE Trans. Microw. Theory Tech.*, 2006, **54**, (2), pp. 788–796
[23] Thiel, C.W.: 'Four-Wave mixing and its applications', Montana State University. Available at http://staff.mbi-berlin.de/bfreyer/fwmixing.pdf, accessed on 8 June 2016
[24] Marciu, D.: 'Optical limiting and degenerate four-wave mixing in novel fullerenes'. PhD thesis, Department Physics, Virginia Polytechnic Institute and State University, Blacksburg, Virginia, 1999
[25] Soldo, M., Gibbons, N., Giuliani, G.: 'Generation of a narrow linewidth mm-wave signal from two phase-locked DFB lasers that are mutually coupled via four wave mixing'. Proc. European Conf. on Lasers and Electro-Optics and the European Quantum Electronics Conf., Munich, Germany, 2009, pp. 77–78
[26] Minch, J.R., Chang, C.-S., Chuang, S.-L.: 'Wavelength conversion in distributed-feedback lasers', *IEEE J. Sel. Top. Quantum Electron.*, 1997, **3**, (2), pp. 569–576
[27] Zanola, M., Soldo, M., Strain, M.J., *et al.*: 'Integrated monolithic device with three mutually coupled DFB lasers for the generation of a tunable narrow linewidth mm-wave signal'. Proc. SPIE, Semiconductor Lasers and Laser Dynamics IV, Brussels, Belgium, April 2010, vol. 7720
[28] Boyd, R.: '*Nonlinear optics*' (Academic Press, Cambridge, MA, 2008, 3rd edn.)
[29] Duchesne, D., Ferrera, M., Razzari, L., *et al.*: 'Nonlinear optics in doped silica glass integrated waveguide structures', in Pal, B. (Ed.): '*Frontiers in guided wave optics and optoelectronics*' (InTech, London, 2010), pp. 269–294
[30] Agrawal, G.P.: 'Four-wave mixing and phase conjugation in semiconductor laser media', *Opt. Lett.*, 1987, **12**, (4), pp. 260–262
[31] Wright, M.W., McInerney, J.G.: 'Injection locking semiconductor lasers with phase conjugate feedback', *Opt. Commun.*, 1994, **110**, (5-6), pp. 689–698
[32] Peters-Flynn, S., Spencer, P.S., Sivaprakasam, S., *et al.*: 'Identification of the optimum time-delay for chaos synchronization regimes of semiconductor lasers', *IEEE J. Quantum Electron.*, 2006, **42**, (4), pp. 427–434
[33] Peters-Flynn, S., Pierce, I., Spencer, P.S., *et al.*: 'Synchronisation recovery in unidirectionally coupled semiconductor lasers', *IEE Proc., Optoelectron.*, 2006, **153**, (1), pp. 8–12
[34] Lang, R., Kobayashi, K.: 'External optical feedback effects on semiconductor injection laser properties', *IEEE J. Quantum Electron.*, 1980, **QE-16**, (3), pp. 347–355

8 Appendix

Continuing from (3) the nonlinear polarisation may be represented as [28]

$$\tilde{P}^{(3)}(t) = \sum_n P(\nu_n)\, \mathrm{e}^{-\mathrm{i}2\pi\nu_n t}. \tag{9}$$

Considering the positive frequencies, the nonlinear polarisation for each can be written as [28]

$$\begin{aligned}
P(\nu_1) &= \epsilon_0\chi^{(3)}(3E_1E_1^* + 6E_2E_2^* + 6E_3E_3^*)E_1,\\
P(\nu_2) &= \epsilon_0\chi^{(3)}(6E_1E_1^* + 3E_2E_2^* + 6E_3E_3^*)E_2,\\
P(\nu_3) &= \epsilon_0\chi^{(3)}(6E_1E_1^* + 6E_2E_2^* + 3E_3E_3^*)E_3,\\
P(3\nu_1) &= \epsilon_0\chi^{(3)}E_1^3,\\
P(3\nu_2) &= \epsilon_0\chi^{(3)}E_2^3,\\
P(3\nu_3) &= \epsilon_0\chi^{(3)}E_3^3,\\
P(\nu_1+\nu_2+\nu_3) &= 6\epsilon_0\chi^{(3)}E_1E_2E_3,\\
P(\nu_1+\nu_2-\nu_3) &= 6\epsilon_0\chi^{(3)}E_1E_2E_3^*,\\
P(\nu_1+\nu_3-\nu_2) &= 6\epsilon_0\chi^{(3)}E_1E_3E_2^*,\\
P(\nu_2+\nu_3-\nu_1) &= 6\epsilon_0\chi^{(3)}E_2E_3E_1^*,\\
P(2\nu_1+\nu_2) &= 3\epsilon_0\chi^{(3)}E_1^2E_2,\\
P(2\nu_1+\nu_3) &= 3\epsilon_0\chi^{(3)}E_1^2E_3,\\
P(2\nu_2+\nu_1) &= 3\epsilon_0\chi^{(3)}E_2^2E_1,\\
P(2\nu_2+\nu_3) &= 3\epsilon_0\chi^{(3)}E_2^2E_3,\\
P(2\nu_3+\nu_1) &= 3\epsilon_0\chi^{(3)}E_3^2E_1,\\
P(2\nu_3+\nu_2) &= 3\epsilon_0\chi^{(3)}E_3^2E_2,\\
P(2\nu_1-\nu_2) &= 3\epsilon_0\chi^{(3)}E_1^2E_2^*,\\
P(2\nu_1-\nu_3) &= 3\epsilon_0\chi^{(3)}E_1^2E_3^*,\\
P(2\nu_2-\nu_1) &= 3\epsilon_0\chi^{(3)}E_2^2E_1^*,\\
P(2\nu_2-\nu_3) &= 3\epsilon_0\chi^{(3)}E_2^2E_3^*,\\
P(2\nu_3-\nu_1) &= 3\epsilon_0\chi^{(3)}E_3^2E_1^*,\\
P(2\nu_3-\nu_2) &= 3\epsilon_0\chi^{(3)}E_3^2E_2^*,
\end{aligned} \tag{10}$$

where $'*'$ denotes complex conjugation.

In each case shown in (10), the frequency argument of P is equal to the sum of the frequencies associated with the field amplitudes that can be seen on the right-hand side (RHS) of the equation, adhering to the convention that a negative frequency is to be associated with a field amplitude that appears conjugated [28]. It should also be noted that the numerical factors of 1, 3 or 6 that are apparent in each term on the RHS of each equation corresponds to the number of distinct permutations of the field frequencies that contribute to that term [1, 28].

Of these many components, the last two, $P(2\nu_3-\nu_1) = 3\epsilon_0\chi^{(3)}E_3^2E_1^*$ and $P(2\nu_3-\nu_2) = 3\epsilon_0\chi^{(3)}E_3^2E_2^*$, are chosen because these are the only frequency components similar in frequency to ν_1 and ν_2, and where the fields are conjugated in both terms, hence this is the so-called phase conjugate injection [1].